VOL. 13, NO. 24, DECEMBER 2018 ISSN 1819-6608
ARPN Journal of Engineering and Applied Sciences

www.arpnjournals.com

THE EFFECTS OF VORTEX SHEDDING ON THE AERODYNAMIC PERFORMANCE OF AIRFOILS

Esther Rami Sikien, Aslam Abdullah, Mohd Fadhli Zulkafli and Mohammad Zulafif Rahim
Department of Aeronautical EngineeringFaculty of Mechanical and Manufacturing Engineering, Universiti Tun Hussein Onn Malaysia, Parit Raja, Batu Pahat, Johor, Malaysia
E-Mail: aslam@uthm.edu.my

ABSTRACT

This is a comparative study involving various National Advisory Committee for Aeronautics (NACA) airfoils NACA 0012, NACA 0024, NACA 4412 and NACA 4424. The numerical simulation involves the air flow passing these models at high Reynolds number and various angles of attack. The study focuses mainly on the aerodynamic performance as represented by lift and drag coefficients. The Computational Fluid Dynamics simulation has been carried out in order to understand the phenomena of vortex shedding. The aim is to investigate the effects of vortex shedding on the aerodynamic performance of airfoils which has still been widely discussed over the years. The methodology has been validated; by using Spalart-Allmaras, K-epsilon and inviscid models, the first with the turbulence intensity and backflow of 0.10% contributed to relatively accurate result. The outcome reveals that there are few aspects that need to be considered in order to control or delay vortex shedding phenomena such as thickness-to-chord ratio, airfoil types, Reynolds number and whether or not it involves transient flow.

Keywords: vortex shedding, lift coefficient, drag coefficient, CFD, airfoil, spalart-allmaras, K-epsilon, inviscid flow, stall.

INTRODUCTION

Aerodynamic force fluctuations usually occur in fluid dynamic system due to vortex shedding. Vortex shedding is defined as fluctuating flow that takes place when fluid (air or water) passing over a bluff body at some definite velocities relying on the size and shape of the body. The process of vortex shedding phenomenon has been the subject of many researches. Even after years of efforts, it has still been a challenging issue in fluid dynamics.

Basically, the starting of vortex-sheet formation is an interaction between two separating shear layers. Once develops, vortex will continue to grow and move circularly from its connected shear layer. In some cases, it is shed downstream. The stability of vortex sheet was theorized by von Karman who argued that it is possible to stabilize vortex shedding if the vortices are shed alternately [1].

Due to the significance of vortex shedding, few related design modifications have been made. One of them involved customizing wing sections to ensure improvement in aerodynamic performance. The presence of sharp edges on a bluff body is also important in improving the accuracy and consistency of the vortex shedding phenomenon. [2]. A body with sharp corner helps in clearing shedding of vortices, and results in high turndown ratio.

The vortex shedding process has been deeply studied by many researches [3], [4] and [5]. Eventually, it is an unsteady flow that takes place at certain range of velocities based on the geometry of the aerodynamic body.

There are two important properties involved in vortex shedding which is Reynolds number of the fluid flow and also the viscosity of the fluid passing over a bluff body. Although many studies on vortex shedding have been involving cylinders, the unsteady wake of fixed airfoils have also been experimentally studied in the presence of shear layer separation and vortex shedding at both high and low *Re* [6], [7] and [8]. Note that the *Re* relates inertial forces to the viscous forces of fluid. For higher *Re*, viscous force less dominates the flow and therefore turbulence easily occurs, whereas for low *Re*, the viscous force dominates and laminar flow is thus developed. In the case of relatively high *Re*, the strong oscillations lead to the formation of a Karman Vortex Street.

There have been numerous intensive researches done in order to control vortex shedding. Such control is necessary due to, for instance, the shedding of vortices from alternate sides of bluff bodies is correlated with strong periodic transverse forces that can damage the body. Thus, suppression of vortex-induced vibrations is required. In some occasions, however, the shedding leads to reduction of drag, which is the desired feature in many applications [9].

In the case of circular cylinder, the vortex formation continues growing as long as it is fed by circulation from the separated shear layer [10]. Cases related to other shapes as aircraft wings contribute limited knowledge on vortex shedding.

This study investigates the effects of vortex shedding on the airfoil of aerodynamic performance by means of numerical simulation.

ANALYSIS

The effects of vortex shedding on the various types of airfoil were observed in ANSYS simulations. NACA 0012 was used to simulate different validation results with different model setups. Simulation results acquired were compared with the result from xfoil predictions. The purpose of running various turbulence models was to ensure the reliability of the method. Three different models used were viscous model of K-epsilon, Spalart-Allmaras and also inviscid model.

Geometry and parameter setup

As shown in Figure-1, there are 4 different geometries of interest, particularly 2 symmetrical airfoils (i.e. NACA 0012 and NACA 0024) as well as 2 unsymmetrical airfoils (i.e. NACA 4412 and NACA 4424). The airfoils point data files that were utilized in this study were taken from [11]. The airfoils are different from each other in terms of their geometries and thickness. This can be observed from the NACA code itself. The last two digits indicate the thickness-to-chord ratio (in percent). Hence, NACA 0012 and NACA 4412 have 12% thickness-to-chord ratio. On the other hand, NACA 0024 and NACA 4424 both have the same 24% thickness-to-chord ratio. Each airfoil was considered at different angles of attack in order to observe the variation in velocity contour and lift coefficient. Thus the stall angle of attack and the vortex shedding formation can be determined and detected, respectively. The problem set up and solution method with respect to turbulence models are shown in Table-1 and Table-2, respectively.

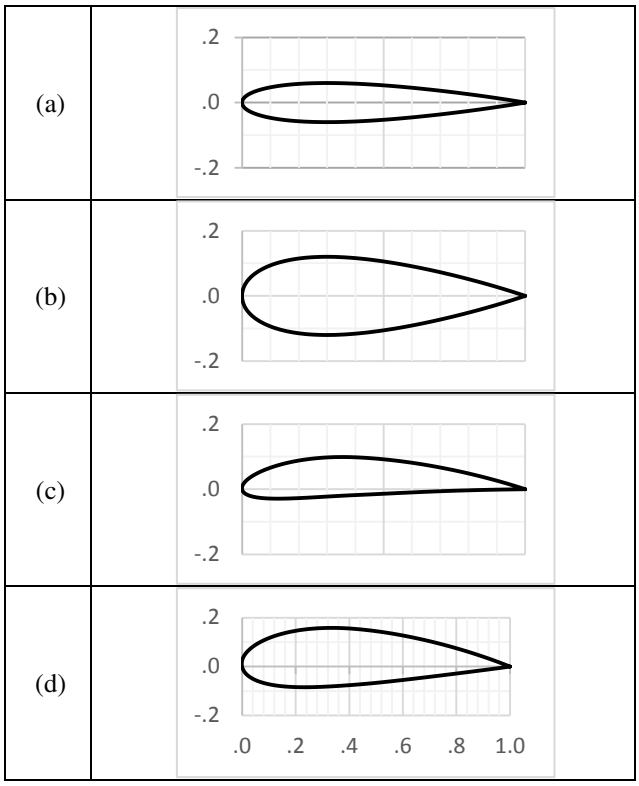

Figure-1. Geometry of airfoils (a) NACA 0012 (b) NACA 0024 (c) NACA 4412 (d) NACA 4424.

Meshing

The hexahedral mesh was used in the simulation. One of the mesh type advantages is that only less element needed for accurate solution. Thus, the solution time would be faster. Advanced size function was set as 'Proximity and Curvature' such that the value of maximum face size could be set manually. Such function would also contribute to a much better mesh which adequately captures all the relevant features. The rest of the parameters were set as default. The mesh is shown in Figure-2.

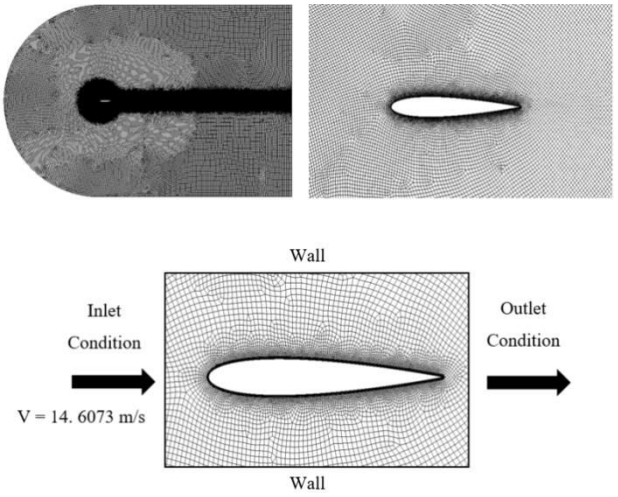

Figure-2. Grid applied for airfoil moving in unbounded flow.

RESULTS AND DISCUSSIONS

Method validation

The lift coefficient C_l profile changes over the time depending on the airfoil geometries. Various parameter combinations have been used in order to validate the data of NACA 0012. Both viscous and inviscid cases were considered. The turbulence models of K-epsilon and Spalart-Allmaras were used in the case of viscous flow. Figure-3 shows the curves of lift coefficient at various angles of attack for three models and against reference data. At low-to-moderate angles of attack, lift coefficient varies quite linearly with angle of attack, α. All the models have a good agreement with the reference data, except for inviscid model where C_l is almost linearly proportional to the angle of attack up to $\alpha = 20°$. Thus, inviscid model is not suitable for reproducing the same data as the reference [12]. By way of contrast, Spalart-Allmaras turbulence model produces the same C_l behaviour as that of reference data such that the error is the lowest. This turbulence model is a simple one-equation model that models the kinematic eddy (turbulent) viscosity, is specifically designed for aerospace application, and it gives good results for boundary layers [13].

Once Spalart-Allmaras model was selected, it was tested using 3 different values of turbulence intensity and backflow which were 0.1%, 2.5%, and 5%.

Figure-4 shows the C_l profiles with respect to turbulence intensity and backflow. In general, the curves are similar to that of the reference data.

Table-1. Parameters setup for three types of model.

SETUP			
Model	**Spalart-Allmaras**	**K-epsilon**	**Inviscid**
Solver	**Pressure Based**		**Density Based**
Velocity Formulation	Absolute		
Time	Steady		
2D Space	Planar		
Model			
Energy	On	Off	On
Model	Spalart-Allmaras (1 equation.)	K-epsilon	Inviscid
	Spalart-Allmaras Production: Strain/Vorticity based	K-epsilon model : Standard	
		Near wall treatment: Standard wall function	
Material Selection			
Air	Density (kg/m3) = Constant (1.225)		
	Cp (Specific Heat) (j/kg-k) = Constant (1006.43)		*Cp* (Specific Heat) (j/kg-k) = Constant (1006.43)
	Thermal Conductivity (w/m-k) = 0.0242		
	Viscosity (kg/m-s) = 1.7894e-05		
Boundary Condition			
Free	Type : Wall		Type : Wall
	Wall Motion = Stationary Wall		
	Shear Condition = No Slip		
	Roughness Height (m) = 0 (Constant)		
	Roughness Constant = 0.5 (Constant)		
Inlet	Type : Velocity-inlet		
	Velocity Specification Method = Magnitude and Direction		
	Reference Frame = Absolute		
	Velocity Magnitude (m/s) = 14.6073		
	Supersonic/Initial Gauge Pressure (pascal) = 0		
	X-Component of Flow Direction = 1		
	Y-Component of Flow Direction = 0		
	Turbulence:		
	Specification Method = Intensity and Length Scale		
	Turbulent Intensity (%) = 0.1%		
	Turbulent Length Scale (m) = 1		
Outlet	Type : Pressure-outlet		
	Gauge Pressure (Pascal) = 0		
	Backflow Direction Specification Method = Normal to Boundary		
	Turbulence:		
	Specification Method = Intensity and Length Scale		
	Backflow Turbulent Intensity (%) = 0.1		
	Backflow Turbulent Length Scale (m) = 1		

Table-2. Solution methods.

SOLUTION METHODS			
Model	**Spalart-Allmaras**	**K-epsilon**	**Inviscid**
Pressure-Velocity Coupling			**Formulation**
Scheme : Coupled			Implicit
			Flux type : Roe-FDS
Spatial Discretization			
Gradient	Least Squares Cell Based		
Flow			Second Order Upwind
Pressure	Second Order		
Momentum	Second Order Upwind		
Modified μ_t	Second Order Upwind		
Energy	Second Order Upwind		
k		Second Order Upwind	
ε		Second Order Upwind	
Solution Controls			
Flow Courant Number : 200			Courant number : 5
Explicit Relaxation Factors :			
Momentum = 0.5			
Pressure = 0.5			
Under-Relaxation Factors :			
Density = 1			
Body Forces =1			
Modified μ_t = 0.8			
μ_t = 1			
Energy = 1			
Monitors			
Residuals, Statistic and Force Monitors	Create: Drag		
	Wall Zones = Part_1 & Part_2		
	Options : Print to Console and Plot		
	Window = 2		
	Average Over = 1		
	Force Vector : X =1, Y=0		
	Create : Lift		
	Wall Zones = Part_1 & Part_2		
	Options : Print to Console and Plot		
	Window = 3		
	Average Over = 1		
	Force Vector : X =0, Y=1		
Solution Initialization			
Method	Standard Initialization		
Compute frm.	Inlet		
Ref. Frame	Relative to Cell Zone		
Initial Values	Gauge Pressure (Pascal) = 0		
	X Velocity (m/s) = 14.6073		
	Y Velocity (m/s) = 0		
	μ_t= 0.001610119	k = 3200598x10^{-10}	T (K) = 300
	T (K) = 300	ε_t = 5.725939e-6	
Run Calculation			
Number Iterations = 3700			

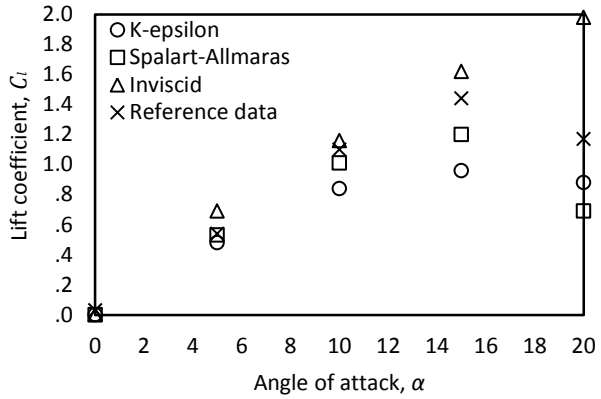

Figure-3. The lift coefficient, C_l profile.

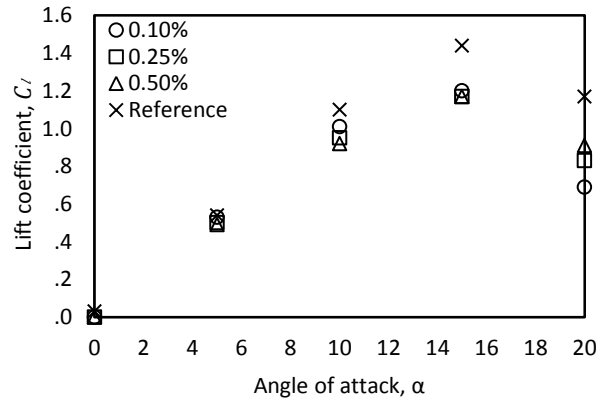

Figure-4. Comparison of C_l profiles with respect to turbulence intensity and backflow.

The lift coefficient profile in the case of 0.10% turbulence intensity is the closest to that of reference data; at $\alpha = 5^o$, $C_l = 0.53$ with only -1.85% error. The lift coefficient increases with angle of attack until it reaches the maximum.

The rest of the cases show greater errors compared to the previously mentioned. For instance, at $\alpha = 5^o$, C_l are 0.50 and 0.49 in the case of 2.5% and 5% turbulence intensity, respectively. This obviously shows greater errors.

Vortex shedding analysis

The velocity contour at stall angle of attack (i.e. on the left of the figure) and the vortex shedding (i.e. on the right of the figure) following the stall are shown in Figure-5. Since steady state solver was applied, the initially transient flow evolved into a steady flow. Theoretically, stall occurs when C_l is maximum, and vortex shedding begins right after the flow separation.

The velocity contours in the case of vortex shedding illustrate that the flow no longer follows the contour of the body (i.e. airfoil) at certain α. This shows that the flow has fully separated. Additionally, it can be seen that the surrounding airstream velocity is very much higher than that of the airflow in the vicinity of each airfoil. Note that the bottom surface pressure distribution does not affect the separation. Two major consequences of the flow separations are a drastic loss of lift (i.e. stalling), and a major increase in pressure drag.

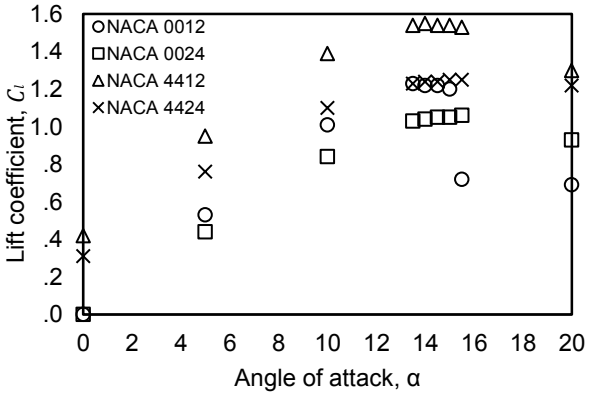

Figure-5. Diversity of lift coefficient for different airfoils at different angle of attack.

The lift coefficients for all four airfoils of interest are given in Figure-6. It is clear that at $\alpha = 0^o$, the lift coefficient is the same for all symmetrical airfoils where $C_l = 0$. Also, the C_l profile of NACA 0012 is greater than that of NACA 0024, in general.

The C_l profile of NACA 4412 is more 'curvy' in comparison to that of NACA 4424. Moreover, C_l profile of NACA 4412 is higher.

In Table-3 the exact stall angle of attack and α when vortex shedding occurs are shown for each airfoil. The value of α is accurate to ±0.5°. Since both symmetrical airfoils have less thickness, the stall occurs relatively earlier. Obviously, the location where vortex shedding first occurs is the trailing edge. Such occurrence vanishes when the steady state condition is achieved.

Vortex shedding was captured at $\alpha = 16^o$, 2.5^o after stall for NACA 0012. Another symmetric airfoil case reveals that vortex shedding was captured $\alpha = 22^o$; the formation is delayed for 6.5^o after stall. As far as unsymmetrical airfoils are concerned, the formation is captured at $\alpha = 18^o$ and 20^o for NACA 4412 and NACA 4424, respectively.

Both the lift and drag coefficient values when the vortex shedding takes place are presented in Table-4. The lift-to-drag ratio l/d = 10.7 for NACA 0012 in comparison to l/d = 5.12 for NACA 0024 (i.e. differ by approximately 50%). Meanwhile, l/d = 11.83 and l/d = 11.09 for both unsymmetrical airfoils NACA 4412 and NACA 4424, respectively. This shows that an airfoil with less thickness gives greater l/d even in the presence of vortex shedding.

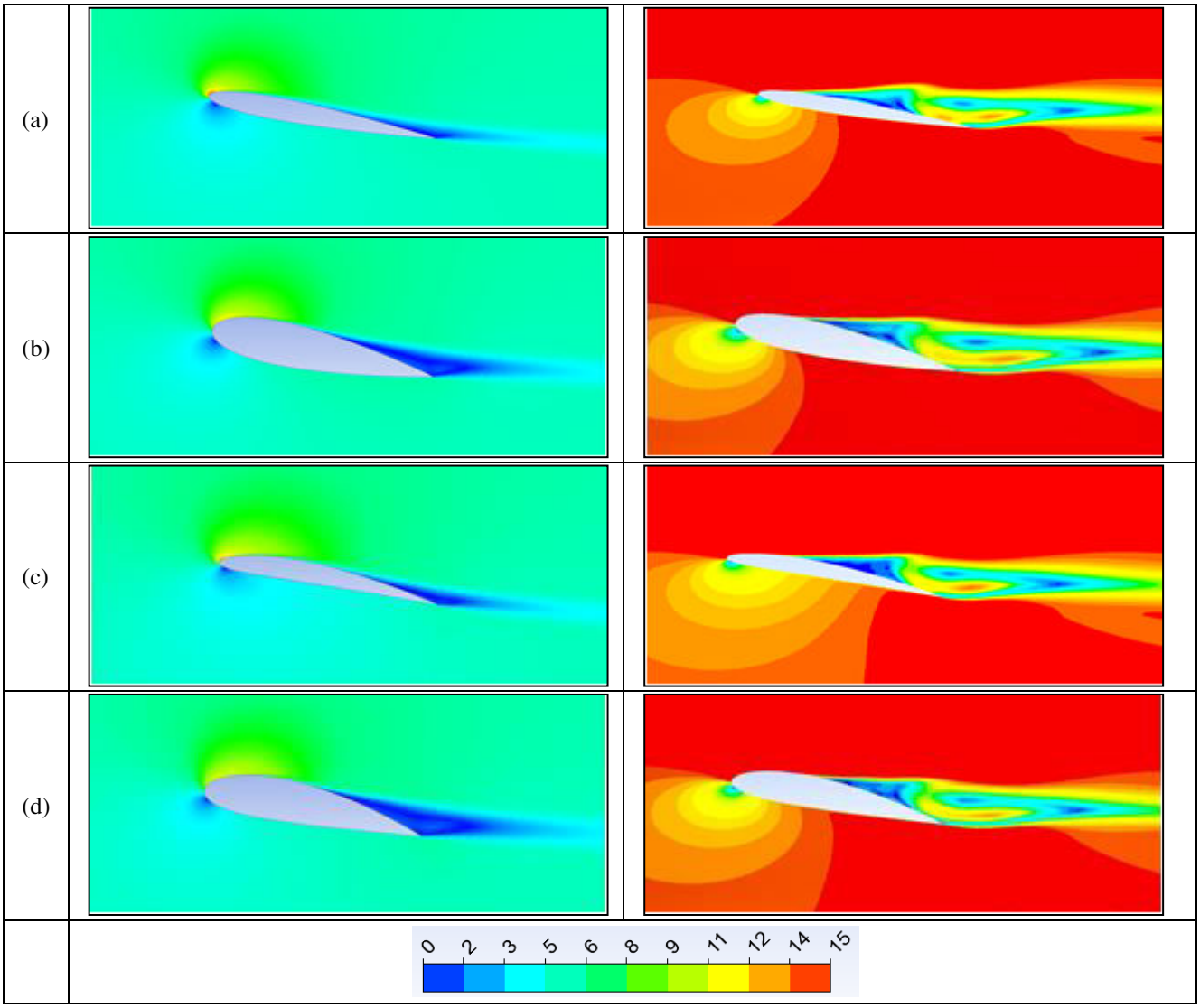

Figure-6. Velocity contour in m/s at α (a) NACA 0012 (b) NACA 0024 (c) NACA 4412 (d) NACA 4424.

Table-3. Occurrence of vortex shedding and stall.

Airfoils	Angle of attack, α		Location of first vortex shedding occurrence
	Stall	Vortex shedding	
NACA 0012	13.5°	16°	Trailing edge
NACA 0024	15.5°	22°	Trailing edge
NACA 4412	14°	18°	Trailing edge
NACA 4424	15°	20°	Trailing edge

CONCLUSIONS

The main purpose of this study is to investigate the effects of vortex shedding on the airfoil aerodynamic performance as represented by lift and drag coefficients. NACA airfoils were selected based on their thickness and whether or not they are symmetrical. The approach of

Table-4. The relationship between the angle of attack when vortex shedding occurs and aerodynamic performance.

Type of NACA	Lift coefficient, C_l	Drag coefficient, C_d
NACA 0012	1.07	0.10
NACA 0024	0.87	0.17
NACA 4412	1.42	0.12
NACA 4424	1.22	0.11

numerical simulation with steady state solver has been taken. The Reynolds number of 1,000,000 with uniform velocity of 14.6073 m/s were adopted.

Lift-to-drag ratio coefficient is higher for unsymmetrical airfoil than that for symmetrical airfoil even when vortex shedding presents. By increasing the angle of attack α, the energy of vortex shedding significantly appears. High *l/d* is typically one of major goals in designing wings. Since an aircraft's required lift depends on its weight, delivering lift with lower drag directly leads to smaller fuel consumption, and better climb performance and glide ratio.

The way vortex shedding influences airfoils' performance can be seen in the context of airfoil geometries as their thickness, positions of both camber and chord lines, and whether or not they are symmetrical. Although vortex shedding cannot be totally prevented, it can be minimised or delayed.

The extension of this study would be, for example, the study of factors that influence the vortex shedding, as in the case of airfoils experiencing ground effects [14], [15], as well as the airfoils in compressible and flows [16], [17].

Important aspects to consider in vortex shedding control mechanism

The study provides information on how and when vortex shedding occurs. First, thickness to chord ratio of an airfoil has been examined; vortex shedding in the case of airfoil with lower thickness-to-chord ratio takes place earlier.

Another aspect is regarding the types of airfoil. It is understood that vortex shedding happens after stall. Since stall happens relatively early for unsymmetric type of airfoils, so does the vortex shedding.

Moreover, smaller *Re* tends to delay vortex shedding. Thus the parameter could be taken into account in the control mechanism of vortex shedding.

ACKNOWLEDGEMENT

The author would like to thank Universiti Tun Hussein Onn Malaysia (UTHM) and Ministry of Higher Education of Malaysia (MoHE) for the research facilities.

REFERENCES

[1] Zobeiri A., Ausoni P., Avellan F. and Farhat M. 2009. Vortex shedding from blunt and oblique trailing edge hydrofoils. 3rd IAHR Int. Meet. Workgr. Cavitation Dyn. Probl. Hydraul. Mach. Syst. 3: 245-252.

[2] Gandhi B. K., Singh S. N., Seshadri V. and Singh J. 2004. Effect of bluff body shape on vortex flow meter performance. Indian J. Eng. Mater. Sci. 11: 378-384.

[3] Ordia L., Venugopal A., Agrawal A. and Prabhu S. V. 2013. Influence of after body shape on the performance of blunt shaped bodies as vortex shedders. Int. J. Mech. Mechatronics Eng. 7: 836-841.

[4] Ausoni P. 2009. Turbulent vortex shedding from a blunt trailing edge hydrofoil. 189.

[5] Azman R. B. 2008. Study of vortex shedding around bluff body using air flow test rig.

[6] Villegas A. and Diez F. J. 2016. Effect of vortex shedding in unsteady aerodynamic forces for a low Reynolds number stationary wing at low angle of attack. J. Fluids Struct. 64: 138-148.

[7] Mittal S. and Raghuvanshi A. 2001. Control of vortex shedding behind circular cylinder for flows at low Reynolds numbers. 2001. Int. J. Numer. Methods Fluids. 35: 421-447.

[8] Taylor Z. J., Gurka R. and Kopp G. A. 2014. Effects of leading edge geometry on the vortex shedding frequency of an elongated bluff body at high Reynolds numbers. J. Wind Eng. Ind. Aerodyn. 128: 66-75.

[9] Tang S. and Aubry A. 2001. Suppression of vortex shedding inspired by a low-dimensional model. J. Fluids Struct. 16: 399-413.

[10] Liu Z. and Kopp G. A. 2012. A numerical study of geometric effects on vortex shedding from elongated bluff bodies. J. Wind Eng. Ind. Aerodyn. 101: 1-11.

[11] Inc T. D. 2017. Airfoil tools. Tucows Domains Inc. http://airfoiltools.com/.

[12] Anderson J. D. 1991. Fundamental of Aerodynamics.

[13] Sadikin A. *et al.* 2018. A comparative study of turbulence models aerodynamics characteristics of a naca0012 airfoil. 10: 134-137.

[14] Abdullah A., Kamsani M. A. and Abdullah K. 2017. Effect of ground proximity on the flow over STOL CH750 multi-element airfoil. IOP Conf. Series: Materials Science and Engineering. 243: 1-8.

[15] Abdullah A., Yazi M. N., Ghafir M. F. A., Mohd S. and Rahim M. Z. 2017. Ground proximity effect on the flow over NACA 4412 multi-element airfoil in clean configuration. IOP Conf. Series: Journal of Physics: Conf. Series. 914: 1-8.

[16] Abdullah A., Jafri M.N.S.M. and Zulkafli M. F. 2017. Numerical study of military airfoils design for compressible flow. ARPN Journal of Engineering and Applied Sciences. 12: 7129-7133.

[17] Abdullah A., Roslan A.A. and Omar Z. 2018. Comparative study of turbulent incompressible flow past naca airfoils. ARPN J. Eng. Appl. Sci. 13: 8527-8530.